Seasonal and spatial variability of CO_2 emission from a large floodplain lake in the lower Amazon

Conrado M. Rudorff,[1] John M. Melack,[1] Sally MacIntyre,[2] Cláudio C. F. Barbosa,[3] and Evlyn M. L. M. Novo[3]

Received 25 February 2011; revised 9 July 2011; accepted 28 July 2011; published 20 October 2011.

[1] The inundation status of the Amazon floodplain affects biogenic gas production and evasion. We analyzed spatial variability of dissolved CO_2 concentration and gas evasion in a large floodplain lake in the lower reach of the Amazon River in four hydrological phases. We calculated surficial CO_2 concentrations from measurements of pH, dissolved inorganic carbon, temperature, and conductivity and used meteorological data to calculate gas transfer coefficients to estimate CO_2 evasion. Gas transfer coefficients that take into account both wind and heating and cooling at the lake's surface are on the order of 10 cm hr^{-1}, approximately four times higher than values previously used in regional estimates of gas evasion from lakes on the Amazon floodplain. Supersaturation of CO_2 occurred throughout the lake and was higher in the littoral zone and in regions receiving Amazon River inflows. CO_2 concentration was reduced in regions with phytoplankton blooms. The range of CO_2 concentrations was least at low water, 47 μM to 233 μM, and largest at high water, 1 μM to 656 μM; the average annual value was 125 μM. We estimate mean (±standard deviation) fluxes from open-water in L. Curuai to the atmosphere of 44 ± 15, 348 ± 13, 371 ± 23, and 364 ± 20 mmol CO_2 m^{-2} d^{-1} during receding, low, rising, and high water, respectively. The error associated with these values reflects, for each hydrological phase, the spatial variation in CO_2 concentration in L. Curuai, a likely range in atmospheric CO_2 levels and temporal variations in gas transfer coefficient within 10-day periods.

Citation: Rudorff, C. M., J. M. Melack, S. MacIntyre, C. C. F. Barbosa, and E. M. L. M. Novo (2011), Seasonal and spatial variability of CO_2 emission from a large floodplain lake in the lower Amazon, *J. Geophys. Res.*, *116*, G04007, doi:10.1029/2011JG001699.

1. Introduction

[2] The Amazon basin stores and cycles a large quantity of carbon, yet *Houghton et al.* [2009] suggest that the region's carbon balance has been, on average, nearly neutral over the last decade. However, there remain uncertainties regarding changes in land use and in the balance between photosynthesis and respiration due to variations in climate. The fluvial system, recently recognized as an important component of the carbon budget, releases to the atmosphere an amount of CO_2 roughly equal to the carbon sequestered by the forest. The basin-wide outgassing of CO_2 from rivers and floodplains was estimated by *Richey et al.* [2002] as 500 Tg C yr^{-1}, but this is considered conservative and is currently under revision [*Richey et al.*, 2009]. Refined analyses of spatial and temporal variations in fluxes are required for uncertainties to be resolved.

[3] Carbon dioxide is supersaturated in most Amazonian rivers and floodplain waters [*Richey et al.*, 1988; *Richey et al.*, 2002] and its exchange with the atmosphere occurs via diffusive and turbulent transfer across the air-water interface [*MacIntyre et al.*, 1995]. On the scale of an individual lake, *Melack and Engle* [2009] reported that CO_2 evasion represented the majority of carbon export. The production of dissolved CO_2 in Amazon floodplains and other tropical wetlands includes respiratory releases from aquatic plants and animals, but is dominated by microbial metabolism [*Hamilton et al.*, 1995; *Waichman*, 1996] which consumes labile organic matter of young age released from seasonally flooded forests, aquatic macrophytes and upland forests [*Quay et al.*, 1992; *Mayorga et al.*, 2005; *Engle et al.*, 2008; *Melack et al.*, 2009; *Richey et al.*, 2009].

[4] The annual flood of the Amazon River influences the ecology and biogeochemistry within its floodplain and plays a major role in retention and transformation of organic matter and exchange of gases between land, water and the atmosphere [*Junk*, 1997; *Melack et al.*, 2009]. *Richey et al.* [1988] measured CO_2 concentration in lakes as part of

[1]Bren School of Environmental Science and Management, University of California, Santa Barbara, California, USA.
[2]Marine Science Institute, University of California, Santa Barbara, California, USA.
[3]Coordenação de Observação da Terra, Instituto Nacional de Pesquisas Espaciais, São José dos Campos, Brazil.

0148-0227/11/2011JG001699

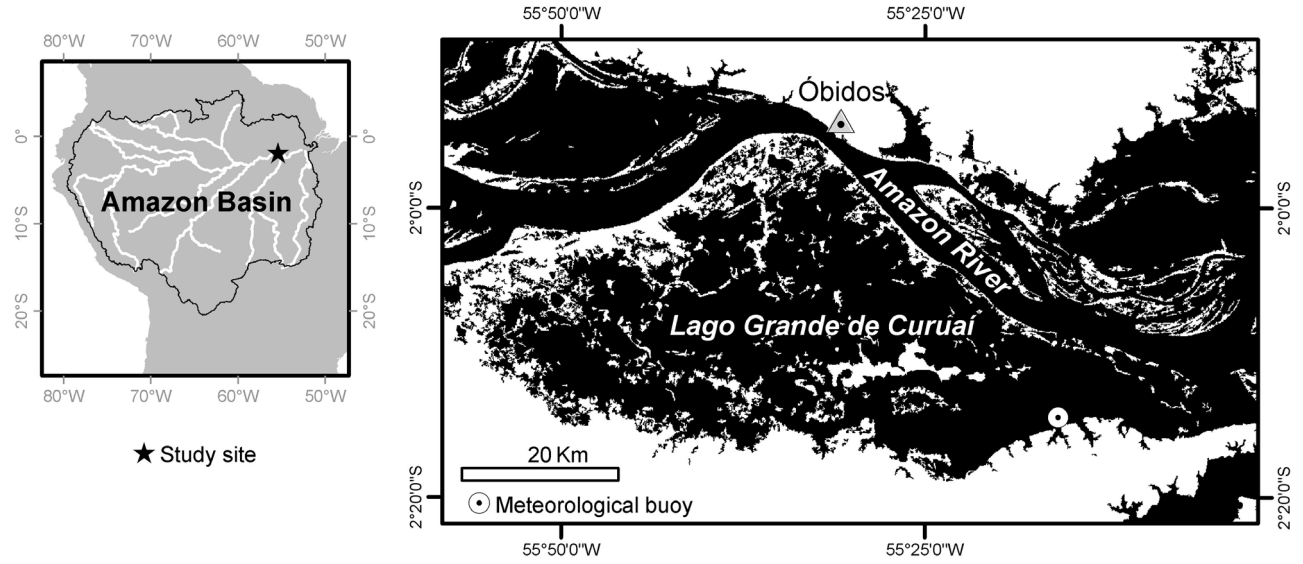

Figure 1. Study site and location of meteorological buoy.

cruises along the Amazon River, but within lake spatial and temporal variability has yet to be examined. Hence, we determined spatial distributions of CO_2 concentration and efflux from open-water of *Lago Grande de Curuai* (Lake Curuai) for four hydrological phases. We calculate surficial CO_2 concentrations from measurements of pH, dissolved inorganic carbon (DIC), temperature, and conductivity and use meteorological data to calculate gas transfer coefficients to estimate CO_2 evasion. The results from our study complement earlier estimates of CO_2 evasion from Amazon floodplains in two important ways: (1) the seasonal and spatial variability in the open-water environment of a large shallow lake system was examined in detail; and (2) samples spanning four hydrological phases were combined with meteorological measurements in the same lake to calculate gas exchanges using wind-based approaches, a surface renewal model and a wind and buoyancy flux based model.

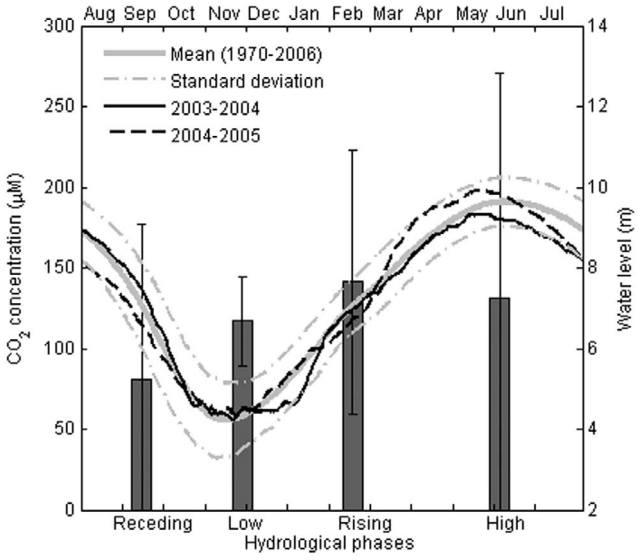

Figure 2. Seasonal variation of spatially averaged CO_2 concentration for four hydrological phases in Lake Curuai. Long-term mean and standard deviation, and 2003–2004 and 2004–2005 hydrographs of the Amazon River at Óbidos, Pará, Brazil.

2. Site Description

[5] *Lago Grande de Curuai* lies in the floodplain of the Amazon River to the south of Óbidos, Pará, Brazil (Figure 1). It is composed of several interconnected lakes temporarily or permanently connected to the Amazon R. by channels and overbank flow. The stage of the Amazon R. varies *ca.* 6 m annually in the nearby reach with a peak in June and minimum in November (Figure 2). The lake's flooded area ranges from about 850 to 2274 km^2; at flood peak open-water covers about 65% of flooded area with flooded vegetation covering the remaining area (Table 1). Water movements and mixing in L. Curuai are complex, and the effects of physical forces (e.g., wind, solar radiation, river inflows) are modified by the

Table 1. Morphological Variables During Hydrological Phases: Flooded Area ($A_{flooded}$); Open-Water Area ($A_{open\text{-}water}$); Mean Depth (z_{mean}) Within Open-Water; and Maximum Depth (z_{max})[a]

	Hydrological Phase		
	High	Receding/Rising	Low
$A_{flooded}$[b] (km^2)	2274	2015	850
$A_{open\text{-}water}$[c] (km^2)	1479	1278	612
z_{mean} (m)	3.2 (2.5)	1.6 (1.5)	0.6 (0.4)
z_{max} (m)	15.0	12.4	9.7

[a]Standard deviations are in parenthesis.
[b]Estimated from digital elevation model obtained by integrated interpolation of bathymetry and Shuttle Radar Topography Mission data [*Barbosa et al.*, 2006; C. Barbosa and C. Rudorff, unpublished data, 2010] and water stage gauged at L. Curuai.
[c]Estimated from classified Landsat images (Barbosa and Rudorff, unpublished data, 2010).

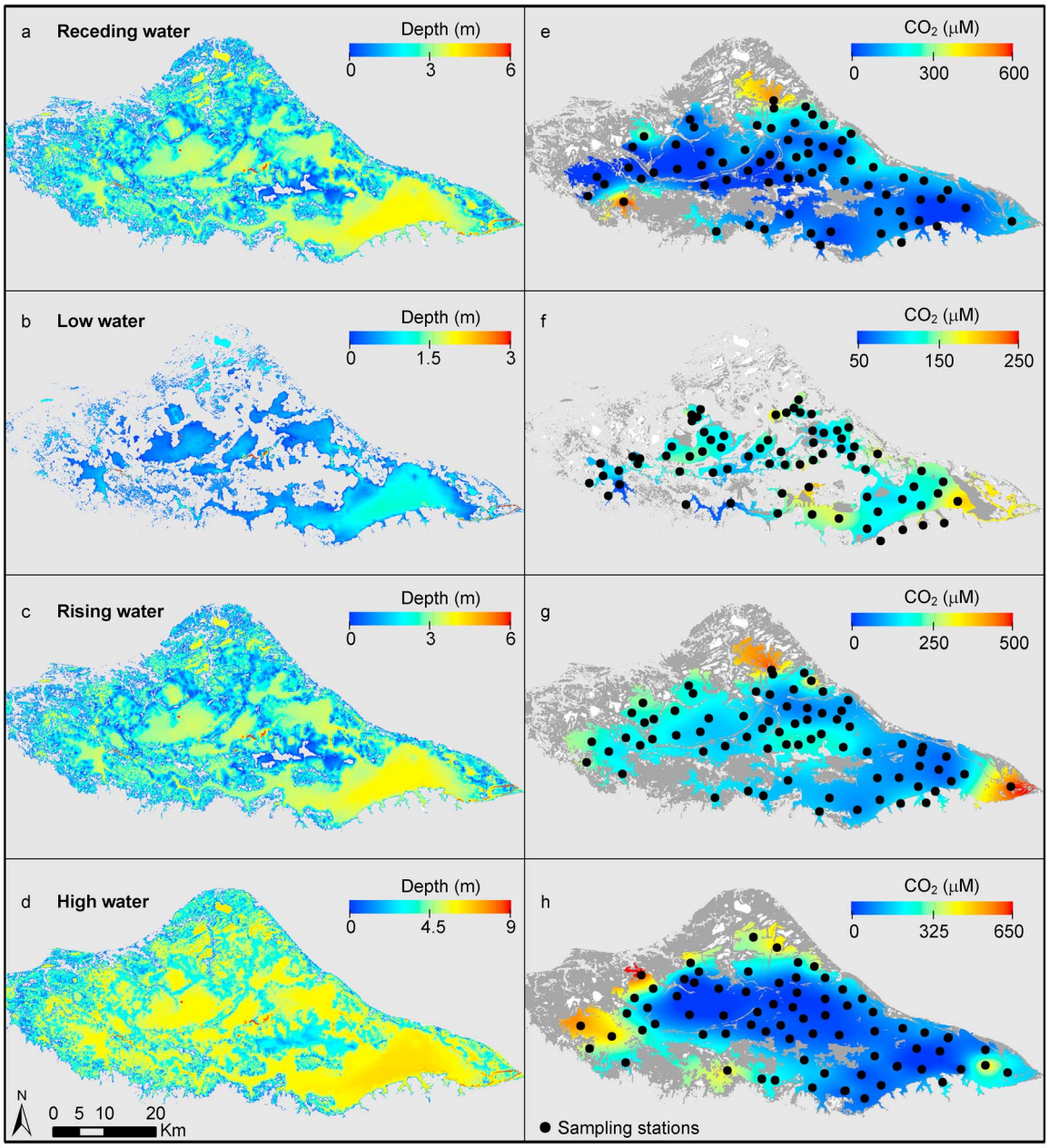

Figure 3. (a–d) Lake bathymetry for four hydrological phases. Images are masked (gray) according to inundation extent. Spatial distribution of dissolved concentration of CO_2 at (e) receding (Sep 2003), (f) low (Nov 2003), (g) rising (Feb 2004), and (h) high water (Jun 2004). Samples were interpolated using a multiquadratic radial basis function. Images are masked according to open-water extent obtained from Landsat image classification. White regions are unsampled isolated lakes. Dark gray regions are differences between inundation and open-water areas and represent flooded vegetation.

lake's surface area and depth, varying seasonally and spatially (Figures 3a–3d and Table 1). During low water the lake becomes sufficiently shallow for sediments to be resuspended by wind-induced turbulence.

[6] *Bonnet et al.* [2008] determined the hydrologic balance for the lake, and reported the lake and its catchment to be, on an annual basis, a source of water to the Amazon R., which accounts for about three quarters of annual inputs of water to the lake. Runoff from the local catchment, direct rainfall, and groundwater seepage were estimated to represent *ca.* 10%, 9%, and 4% of the annual total inputs, respectively. Each year, the storage phase of L. Curuai starts between November and January and lasts until May–June; the drainage phase starts in July and lasts until November.

[7] *Barbosa et al.* [2010] described large seasonal and spatial variations in total suspended sediment (TSS), chlorophyll-*a*, and pH throughout L. Curuai. Average surface water concentrations of TSS changed from 14.5 mg L^{-1} during high water to 463 mg L^{-1} during low water. Average chlorophyll-*a* varied from 8 μg L^{-1} during rising water to

Table 2. Field Campaign Dates and Number of Samples[a]

	Hydrological Phase			
	Receding	Low	Rising	High
Date of Field Campaigns	25 Sep to 7 Oct 2003	22 Nov to 2 Dec 2003	3–12 Feb 2004	3–19 Jun 2004
Samples (n)	71	73	72	74
SD (m)	0.23 (0.11)	0.08 (0.04)	0.10 (0.03)	0.65(0.05)
k_d [b] (m^{-1})	6.6 (2.7)	18.1 (4)	14.7(6.3)	2.0 (0.2)
pH	7.68 (0.75)	6.69 (0.58)	7.25 (0.33)	7.51 (0.76)
DIC (mg L^{-1})	11.8 (2.7)	7.5 (4.0)	16.6 (4.1)	32.3 (3.6)
CO_{2aq} [c] (μM)	92.2 (114.2)	125.2 (34)	148 (85.2)	133 (150.3)
CO_{2aq} [d] (μM)	81.1 (95.6)	116.8 (27.5)	141.5 (81.8)	131 (139)
CO_{2eq} [e] (μM)	11.9 (1.9)	12.2 (1.7)	12.6 (1.9)	12.7 (1.7)

[a]Mean transparency from Secchi disk (*SD*), light attenuation coefficient (k_d), pH, dissolved inorganic carbon (DIC), dissolved CO_2 concentration in surface waters (CO_{2aq}), and dissolved CO_2 concentration in equilibrium with the atmosphere (CO_{2eq}). Standard deviations are in parenthesis.
[b]Estimated using the conversion factor for turbid lakes k_d = 1.3/SD [*Koenings and Edmundson*, 1991].
[c]Estimated from samples.
[d]Estimated from interpolated surfaces (see text).
[e]Temporal variations in atmospheric CO_2 concentrations (S. Miller, unpublished data, 2004) and spatial variation in L. Curuai surface water temperature were used to calculate variability in CO_{2eq}.

70 μg L^{-1} during receding water. While pH in the Amazon R. was relatively constant throughout the year (*ca.* 6.5), pH in the lake varied from an average of 6.7 during low water to 7.7 during receding water. High pH, up to 9.2, was found during receding water in areas with algal blooms of up to 338 μg L^{-1} of chlorophyll-*a*.

3. Methods

3.1. Field Measurements

[8] Four campaigns were conducted to sample limnological parameters during the four phases of inundation: receding (September 2003), low (November 2003), rising (February 2004), and high water (June 2004). Sampling stations were distributed in a dispersed spatial pattern ($P < 0.01$; based on the average nearest neighbor Euclidean distance test) over the main open-water region with average nearest neighbor distance of 3 km (Figure 3 and Table 2). Samples were collected between 1000 and 1400 h over periods of 10 to 16 days. Transparency was measured using a 20-cm diameter Secchi disk. Temperature (accuracy of ±0.3°C), conductivity (accuracy of ±1%), and pH (accuracy of ±0.05) were measured with routinely calibrated Horiba water quality sensors. Water was collected using a cylindrical sampler which integrated the water column from surface to Secchi depth. Water samples were filtered under vacuum through glass fiber filters (Whatman GF/C, 47 mm diameter) and frozen in the field for subsequent laboratory analysis. These manipulations may change DIC concentrations slightly. In the laboratory, concentrations of DIC were determined using a Shimadzu TOC-5000A carbon analyzer calibrated with potassium biphthalate. Further description of sampling strategy and additional parameters measured are provided by *Barbosa et al.* [2010].

[9] Time series measurements of meteorological parameters became available from an instrumented buoy moored in the southeastern region of L. Curuai (Figure 1) in April, 2004. Monitored parameters included water temperature at 1 m depth (shielded thermistors: MEAS 44033RC; accuracy of ±0.1°C), air temperature and relative humidity (Rotronic MP103A; accuracies of ±0.3°C and ±1.5%, respectively), down- and upward shortwave radiation (wavelength range of 400–1100 nm; sensitivity of 490 $\mu V/W/m^2$; accuracy of ±16%), wind speed and direction (R. M. Young 05106; accuracies of ±0.3 m s^{-1} and ±3 degrees, respectively) at 3 m above the lake, and atmospheric pressure (Vaisala PTB100-A; accuracy of ±0.3 mb at 20°C).

[10] Since the high water campaign in June 2004 was the only one with concurrent meteorological data, to approximate conditions during the three other seasons measurements acquired in the corresponding days of the following year were used. The drought at the end of 2005 did not affect our data since it occurred outside of the period of our measurements; the water levels were in good agreement between the periods from mid-2003 to mid-2004 and from mid-2004 to mid-2005. Measurements from the Vila Franca meteorological station [*Fitzjarrald et al.*, 2009], located 20 km to the southeast of the buoy (2° 20′ 55″ S; 55° 1′ 44″ W), indicated that solar radiation and air temperature were on average 18% and 3% higher, respectively, in the period from mid-2004 to mid-2005 compared to mid-2003 to mid-2004. Small gaps in data from L. Curuai buoy station, due to telemetry signal losses, were filled with data from the Vila Franca meteorological station. Longwave radiation emitted from the lake surface was estimated from water temperature according to the Stefan-Boltzmann law with an emission coefficient of 0.97. The downward flux of longwave radiation was obtained as hourly averages from two years (2002 and 2003) measured at the Tapajos National Forest (3° 1′ 5″ S; 54° 58′ 8″ W) [*Miller et al.*, 2009].

[11] Depth of the actively mixing layer (z_{AML}) is required for computation of the gas transfer coefficient using the surface renewal model. This layer is also known as the surface layer and is the layer in direct contact with the atmosphere and thus where heat and momentum are being exchanged [*Imberger*, 1985]. It is generally quantified by slight changes in temperature or by near uniform values of turbulence [*Shay and Gregg*, 1986; *MacIntyre et al.*, 2009]. Values of z_{AML} were assumed to be 0.5 m or the seasonal lake mean depth (z_{mean}) because temperature profiles were not measured. This decision was based on our examination of the frequency and

extent of vertical mixing in Lake Calado, determined from multiyear time series [*Melack and Fisher*, 1983; *MacIntyre and Melack*, 1984, 1988], and the seasonal morphometric changes of L. Curuai (Figures 3a–3d and Table 1). Seasonal stratification persisted once the depth of L. Calado reached about 6 m. During stratification, the mixed layer deepened at night due to cooling and stratified in the day due to heating. Similar patterns are expected in L. Curuai, although wind induced mixing may cause greater mixed layer depths in the larger lake. However, computed attenuation coefficients reach 18 m^{-1} during low water (Table 2); hence daily stratification is likely. At high water, regions deeper than 6 m represent only 16% of open-water, and this portion is insignificant during the other hydrological phases. Based on similarities and differences between L. Curuai and L. Calado, the water column in L. Curuai during the low and medium (rising and receding) water stages is likely to be fully mixed at sunrise, develop a shallow thermocline (~0.5 m) toward midday under low wind conditions, and fully mix again at night. During the high water stage, the lake may develop periods of stable stratification under low wind conditions with significant diel variation of the mixed layer depth (1 to 6 m, depth permitting).

3.2. Calculation of CO_2 Concentrations

[12] Dissociation constants from *Plummer and Busenberg* [1982] and inorganic carbon species as a function of pH from *Stumm and Morgan* [1996] were used for conversion of DIC to dissolved carbon dioxide concentrations in surface waters (CO_{2aq}). Adjustments were made for ionic strength, but without complete major ion data, we estimated ionic strength from conductivity [*Butler*, 1992]; these adjustments were very small because the waters are dilute (mean conductivity of 39 μS with a standard deviation of 10 μS). Atmospheric partial pressures of CO_2 of 430 ± 50 μatm were used in our calculations. Measurements of atmospheric partial pressure of CO_2 over Amazon floodplain lakes are scarce, and we based our values on recent observations by S. Miller (unpublished data, 2004) obtained above the surface of Lago Verde, located 50 km southeast of L. Curuai during high water. The concentration of dissolved CO_2 in equilibrium with the atmosphere (CO_{2eq}) was calculated using Henry's law. For comparison in our discussion, concentrations presented in μatm in the study by *Richey et al.* [2002] were converted to μM, using Henry's constant for CO_2 at 25°C (0.0339 M atm^{-1}) and correcting for the partial pressure of water (0.0313 atm).

3.3. Gas Exchange at the Air-Water Interface

[13] The magnitude and direction of the gas flux is dependent on the concentration difference between the atmosphere and water and upon transport processes at the interface. CO_2 fluxes were calculated using the dissolved CO_2 concentration departure from equilibrium and a gas transfer coefficient (k).

$$F = k\left(CO_{2aq} - CO_{2eq}\right) \tag{1}$$

Due to the uncertainty in parameterizing the gas transfer coefficient, we used three models to determine a range of k values.

[14] The first model (C&C) used is the wind-based approach of *Cole and Caraco* [1998]:

$$k_{600,\,C\&C} = 2.07 + 0.215\ U_{10}^{1.7}, \tag{2}$$

where k_{600} is the gas exchange coefficient normalized to the Schmidt number of CO_2 at 20°C in freshwater (Sc = 600) and U_{10} is the wind speed at a 10 m height above the water surface. Wind measured at 3 m was converted to U_{10} assuming law of the wall scaling and taking into account atmospheric stability.

[15] The second model (SR) used is a small eddy version of the surface renewal model, which takes into account turbulence generated by wind action and heat losses that cause convective motions in the water column [*MacIntyre et al.*, 1995].

$$k_{600,\,SR} = c_1(\varepsilon\nu)^{0.25}, \tag{3}$$

where ν is the kinematic viscosity. We let c_1 = 0.56 [*Isenogle*, 1985]. The coefficient has not yet been fully established and current values range from 0.419 to 1.2 [*Zappa et al.*, 2007; *MacIntyre et al.*, 2010]. The dissipation of turbulent kinetic energy (ε) in the active mixed layer was computed from the water friction velocity (u_{*w}) and buoyancy flux (β).

$$\varepsilon = 0.84\left[0.58(-\beta) + 1.76u_{*w}^3/\kappa z_{AML}\right], \tag{4}$$

where the coefficients were determined empirically [*Lombardo and Gregg*, 1989] and κ is the von Karman constant. u_{*w} is computed from shear stress at the air-water interface assuming it is equal on either side of the interface, giving $\tau_w = \rho_w u_{*w}^2 = \tau_a = \rho_a C_d U^2$ where τ_a and τ_w are shear stress on air and water side of the air-water interface; U is wind velocity at 3 m height and C_d is a drag coefficient computed for that height following *Amorocho and DeVries* [1980]; ρ_a and ρ_w are density of air and water, respectively. The buoyancy flux is calculated as

$$\beta = g\alpha H/\rho_w C_p, \tag{5}$$

where g is gravity, α is the coefficient of thermal expansion, C_p is heat capacity, and H is the effective heat flux.

$$H = S + q(0) + q(z_{AML}) - \frac{2}{z_{AML}}\int_{z_{AML}}^{0} q(z)dz, \tag{6}$$

where $S = \rho_w C_p\ \langle w'T'(0)\rangle$ is the surface heat flux, obtained by the sum of latent heat flux, sensible heat flux, and longwave back radiation; q is shortwave radiation; and z is depth. Light attenuation coefficient (k_d) was estimated based on Secchi disk (SD) measurements using the conversion factor for turbid lakes k_d = 1.3/SD suggested by *Koenings and Edmundson* [1991].

[16] The penetration of radiation into the water column was parameterized using Beer's Law following *Jellison and Melack* [1993]; angle of refraction was included in the calculation.

[17] Following *MacIntyre et al.* [2010], a damping coefficient (c_2/z_{AML}) was introduced to equation (4) to account for the effect of dampening of turbulence during periods of

Table 3. Descriptive Statistics for Dissolved CO_2 Concentration in Surface Waters (CO_{2aq})

	Hydrological Phase			
	Receding	Low	Rising	High
Mean	92.2	125.2	148.0	133.0
Median	61.1	121.5	128.9	81.7
Standard Deviation	114.2	34.0	85.2	150.3
Minimum	0.3	47.1	36.0	1.3
Maximum	608.0	233.0	490.2	656.0
Range	607.7	186.0	454.2	654.7
Interquartile Range	121.3	34.9	99.0	163.9
Skewness	2.352	0.657	2.12	1.529
Kurtosis	7.339	1.453	6.38	1.888

heat gain. Dissipation (equation (4)) was then computed as $\varepsilon = 0.84[0.58(-\beta) + (c_2/z_{AML})1.76u^3_{*w}/\kappa\ z_{AML}]$ when $L_w/z_{AML} \geq 0$ and $U_{10} < 3$ m s^{-1}; where L_w is the water-side Monin-Obukhov length scale. Since data are lacking to determine z_{AML}, the computation was run twice with z_{AML} fixed at 0.5 m and at the seasonal lake mean depth (z_{mean}) which represent the approximate range of diurnal variation expected for L. Curuai (as described above).

[18] The third model (EC) used is a wind-based model that includes diel heating and cooling [*MacIntyre et al.*, 2010].

$$\beta > 0(\text{cooling}), k_{600,\,EC} = -0.15 + 1.74\ U_{10} \quad (7)$$

$$\beta < 0(\text{heating}), k_{600,\,EC} = 2.0 + 2.04\ U_{10} \quad (8)$$

CO_2 exchange coefficients (k) were converted as a function of field conditions based on the Schmidt number (Sc) dependency, assuming $n = 0.5$ which corresponds to the case of turbulent flow below a free surface [*Jähne et al.*, 1987].

$$k_i = k_{600,\,i}(Sc/600)^{-n}, \quad (9)$$

where i is an index representing the different models (C&C; SR; EC).

4. Results

4.1. CO_2 Concentrations and Spatial Patterns

[19] The four hydrological phases had different statistical distributions of CO_2 (Table 3). For low water, the mean and median were nearly equal, the skewness and kurtosis statistics were low, the Kolmogorov-Smirnov test was not significant ($P > 0.01$), and the data fit a normal curve well. For the other three hydrological phases the mean was higher than the median, skewness and kurtosis statistics indicated a disproportionate number of values on the upper tail of the distributions, the Kolmogorov-Smirnov test was significant ($P < 0.01$), and the data fit a normal curve poorly. Hence, the mean was not a good measure of central tendency for these data. Additionally, there were statistical outliers with large values in all four data sets; receding and rising water had extreme CO_2 values 4.5 and 4 standard deviations above the mean, respectively. For all hydrological phases, extreme observations were located in the littoral zone on the perimeter of the sampling stations.

[20] Median values are close to robust estimates of central tendency and indicate receding water as the period of lowest CO_2 concentration (61 μM) and rising water as the highest (129 μM). The median test (Chi-square) was used to determine if CO_2 levels differ among the four hydrological phases. Across all 286 samples, the median CO_2 was 113 μM. Low and rising water had a larger proportion of samples with CO_2 greater than the overall median, while receding and high water had a larger proportion of samples with CO_2 smaller than the median. The Chi-square value was 26.2, and the asymptotic significance was less than 0.01, indicating the existence of an overall effect of seasonality. The Mann-Whitney test was then used to identify seasonal gradients in levels of CO_2. Low water CO_2 levels were significantly greater than the levels at receding water ($P < 0.01$). The transition between low and rising water did not change CO_2 levels significantly. CO_2 concentrations became lower ($P < 0.01$) as water level rose to high water. The change in CO_2 levels was not significant between high and receding water.

[21] Radial basis functions (subtype multiquadratic) were used to interpolate CO_2 spatially within the main open-water body of L. Curuai, as it makes no assumptions about the normality of the data [*Buhmann*, 2003]. Moran's index, I [*Moran*, 1948; *Ripley*, 1981], was used to identify the overall spatial patterns of CO_2 levels. Spatial autocorrelation was significant for all hydrological phases with strong tendency of clustering during receding and rising water ($P < 0.01$) and slightly less for low and high water ($P < 0.10$). Local Moran statistics [*Anselin*, 1995], were then used to identify where high or low values cluster spatially, and occurrences of spatial outliers. CO_2 concentrations in the lake ranged from 0.3 μM to 608 μM during receding water (Figure 3e). Concentration in the Amazon R. (225 μM) did not influence lake waters during this phase of floodplain drainage. The two samples to the west with high values of CO_2 surrounded by low values are spatial outliers ($P < 0.01$). The clustering of high values observed in the northernmost littoral region is statistically significant ($P < 0.01$). At low water, CO_2 concentrations ranged from 47 μM to 233 μM (Figure 3f). CO_2 concentrations increased toward the eastern channels possibly due to the influence of Amazon R. inflow with CO_2 concentration estimated as 495 μM. Two points with indication of high CO_2 clustering ($P < 0.01$) and six points of low CO_2 clustering were observed, and there were no significant spatial outliers. During rising water, CO_2 concentrations ranged from 36 μM to 560 μM (Figure 3g). A cluster of high CO_2 observed in the northernmost littoral region is statistically significant ($P < 0.01$). Clusters of low values were observed in eastern main body of water ($P < 0.01$); the sample furthest to the east with a high value was identified as a spatial outlier ($P < 0.01$). However, Amazon R. inflow from the two main eastern channels, with CO_2 concentration estimated as 595 μM, is likely to be the cause of the high CO_2 concentration observed at this station. During high water, surface concentrations of dissolved CO_2 ranged from 1 μM to 656 μM (Figure 3h). Based on two samples, surface concentrations in the Amazon R. were 372 μM and 425 μM. Amazon R. inflows from western channels and northern overbank flow influenced CO_2 concentration in receiving waters of the floodplain. Statistically significant ($P < 0.01$) clusters of high CO_2 concentrations were observed in the western lit-

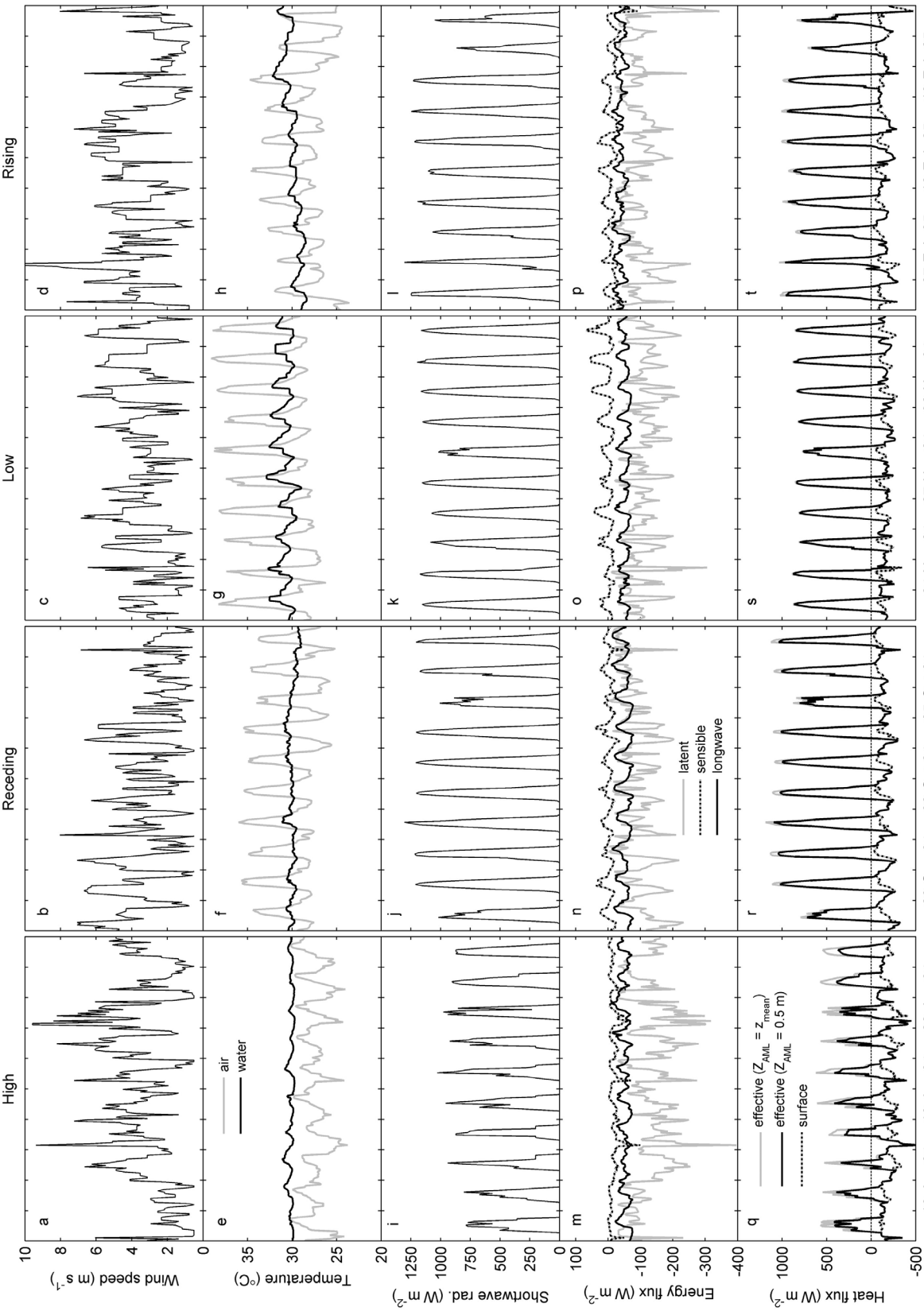

Figure 4. Hourly average values of (a–d) wind speed at 10 m, (e–h) air and 1 m water temperatures, (i–l) net shortwave radiation (400–1100 nm), (m–p) sensible heat, latent heat, and longwave radiation fluxes, (q–t) surface heat flux and effective heat flux, assuming active mixing layer depth equivalent to 0.5 m (z_{AML} = 0.5 m) and the seasonal lake mean depth ($z_{AML} = z_{mean}$).

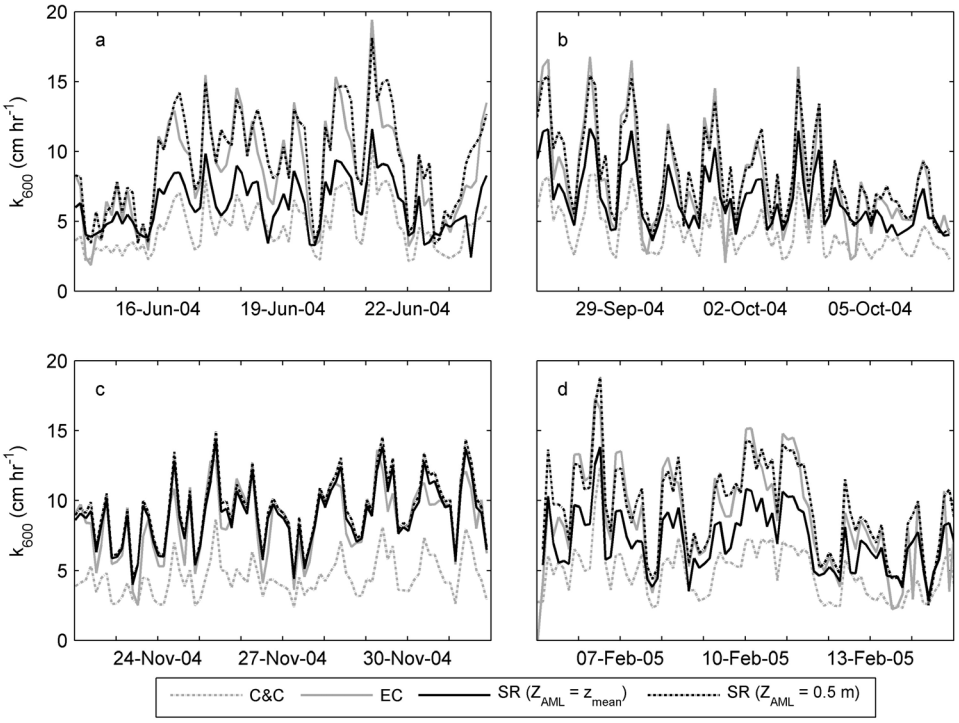

Figure 5. Gas transfer coefficients for (a) high, (b) receding, (c) low, and (d) rising water, displayed as 3 h averages, calculated using: wind-based model following *Cole and Caraco* [1998] (C & C), a wind and buoyancy flux based model (EC), and surface renewal model following *MacIntyre et al.* [2010] assuming active mixing layer depth equivalent to 0.5 m (SR (z_{AML} = 0.5 m)) and the seasonal lake mean depth (SR(z_{AML} = z_{mean})).

toral regions. Significant clusters of low CO_2 were observed in interior pelagic regions. The sample to the east with a high concentration surrounded by low concentrations is a spatial outlier ($P < 0.01$). In this case the high concentration may not be explained by Amazon R. inflow from the eastern channels since at high water the flows in these channels are outward.

4.2. Meteorological Conditions

[22] Ten-day time series of meteorological measurements and computed energy fluxes for the four hydrological phases are shown in Figure 4. Wind generally intensified during daytime and weakened during nighttime, reaching speeds above 5 m s^{-1} on most days (Figures 4a–4d). Ranges of diel variation of water temperature measured at 1 m varied seasonally (Figure 4e–4h). Greater diel variation of water temperature was observed at low water. Toward the end of the rising water period and during high water, air temperature remained lower than water temperature. Maximum net shortwave radiation typically exceeded 1000 W m^{-2} each day, except during June (Figures 4i–4l). Sensible heat flux remained negative during June (Figure 4m), and ranged from about −15 W m^{-2} during nighttime to 20 W m^{-2} during daytime in September (Figure 4n); −15 W m^{-2} during nighttime to 50 W m^{-2} during daytime in November (Figure 4o); and −30 W m^{-2} during nighttime to 40 W m^{-2} during daytime in February (Figure 4p). Net longwave radiation ranged typically from −30 W m^{-2} during nighttime to −70 W m^{-2} during daytime in all periods. Evaporative cooling was substantial, and values of latent heat flux were lower than −200 W m^{-2} during windy periods and when surface water temperatures were higher than the air temperatures.

[23] The effective heat flux, which indicates whether the actively mixing layer will gain or lose heat to the atmosphere, was positive during daytime, indicating that the upper water column tended to stratify at those times, and negative at night indicating mixed layer deepening would occur. The effective heat flux was slightly higher during daytime when z_{AML} was assumed to be z_{mean}, compared to when z_{AML} = $z_{0.5\ m}$, due to the greater volume present to absorb and distribute the heat (Figures 4q–4t). However, the timing of the shift from positive to negative values was independent of the value of z_{AML}, hence the sign of buoyancy flux, which is computed from effective heat flux and is needed for equation (4), was independent of z_{AML}.

4.3. Gas Transfer Coefficients

[24] The lowest estimates of k_{600} were obtained using *Cole and Caraco*'s [1998] wind based model, $k_{600,\ C\&C}$ (Figure 5). Values were on average 85% higher when computed using the regression equations based on wind and buoyancy flux, $k_{600,\ EC}$. Estimates of $k_{600,\ SR}$ with the surface renewal model depended upon the assumed z_{AML}. When using z_{AML} = $z_{0.5\ m}$, $k_{600,\ SR}$ was statistically higher than $k_{600,\ EC}$ ($P < 0.01$; Mann-Whitney test). The slight seasonality observed in both estimates of k_{600} was significant ($P < 0.05$; median test) (Figure 6a). When assuming z_{AML} = z_{mean}, seasonality was more pronounced ($P < 0.01$; median

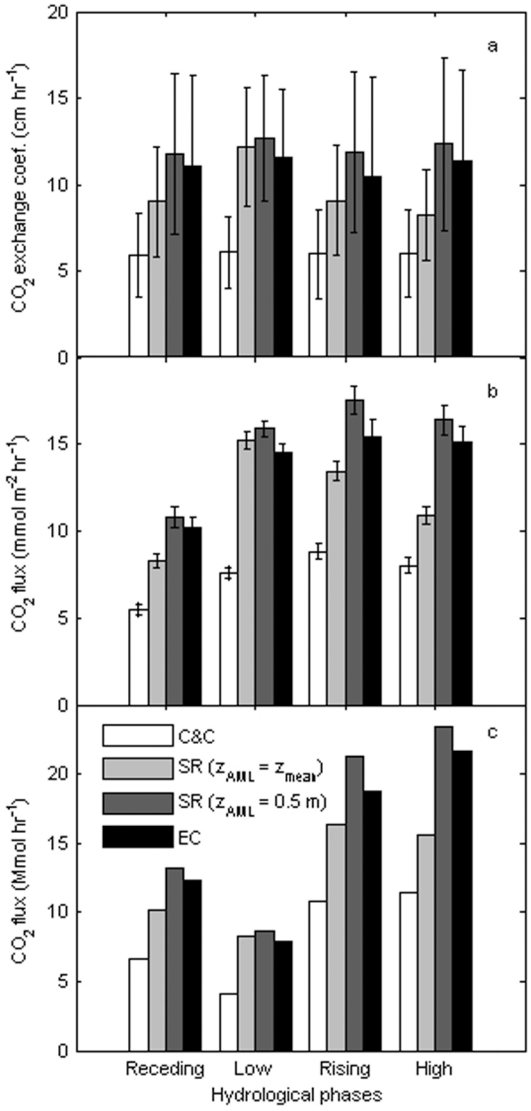

Figure 6. (a) Gas exchange coefficients for CO_2 in Lake Curuai. Mean and standard deviation based on 10-day time series shown in Figure 5. (b) Estimates of CO_2 evasion from lake computed using mean values of CO_2 departure from saturation and gas transfer coefficient. (c) Mean lake seasonal fluxes accounting for the variation in open-water surface area for the four hydrological phases. Legends for Figures 6a and 6c are the same as presented in Figure 6b.

test) with higher estimates obtained during low water and lower estimates during high water.

4.4. Evasion of CO_2

[25] CO_2 evasion from open-water was estimated for each hydrological phase (Figure 6b) using the average values obtained from CO_2 departure from saturation (Table 2; $CO_{2aq} - CO_{2eq}$), and gas transfer coefficients averaged over the 10-day time series (Figure 6a) of each field campaign. Since the averaged gas transfer coefficients computed with the wind based models (C&C and EC) had almost no seasonal variation, their correspondent results of CO_2 evasion shown in Figure 6b reflect the proportions of seasonal average CO_2 concentration (Figure 2). The only clear exception was the estimate of $k_{600,SR}$ assuming $z_{AML} = z_{mean}$; in this situation estimates of areal evasion rate were higher at low water (Figure 6a).

[26] By combining CO_2 flux with the total areal extent of the main body of open-water for each phase (Table 1), the highest rates of evasion, obtained using the wind-based models (C&C and EC), were observed during high water (Figure 6c). In these cases, variation in lake areal extent was the principal determinant of seasonal differences, followed by CO_2 concentration. Seasonal variation caused by changes in gas transfer velocities was important in determining rates of evasion only when using the surface renewal model and assuming $z_{AML} = z_{mean}$. The effect of this model was to reduce overall differences in rate of evasion.

5. Discussion

[27] Open-water surficial concentrations of CO_2, and hence gas evasion, vary in L. Curuai according to the hydrological phase of the Amazon River and distance from shore. Strong gradients of higher CO_2 concentrations were observed toward littoral regions at receding, rising and high water. Significant relations between CO_2 and depth, with Pearson's correlation coefficients of −0.25 ($P < 0.05$), −0.42 ($P < 0.01$), and −0.23 ($P < 0.05$), were observed for these phases, respectively. High CO_2 levels in littoral regions were likely due to increased root respiration associated with floating macrophytes [*Hamilton et al.*, 1995] and decomposition of plant material in the aquatic-terrestrial transition zone during drying and wetting phases. While in some littoral regions CO_2 concentrations reached levels over 600 μM, pelagic regions fell to close to 0 μM during receding and high water when phytoplankton were abundant [*Barbosa et al.*, 2010]. As a result of increased photosynthesis, pH increased with concomitant decreases in CO_2. For example, during receding waters at one offshore station, CO_2 concentration was 0.3 μM, chlorophyll-*a* concentration was 338 μg L^{-1}, and pH was 9.2. Significant correlations between CO_2 and chlorophyll-*a* of −0.39 ($P < 0.01$) and −0.53 ($P < 0.01$) were observed during receding and high water, respectively. Furthermore, diel stratification is likely to develop in pelagic regions and seasonal stratification may develop in regions deeper that 6 m [*Melack and Fisher*, 1983; *MacIntyre and Melack*, 1984, 1988] and limit mixing of water enriched in CO_2 with depleted water in the upper mixed layer. Since samples were collected from surficial water during mid-day heating, values are likely to be lower than at other times of day [*Crill et al.*, 1988]. In particular, higher surficial CO_2 concentrations would be expected during nighttime due to respiration and deep convective mixing.

[28] Spatial pattern of CO_2 concentration at low water was different from the other hydrological phases and likely due to (1) shallow depth (z_{mean} = 0.6 m) and frequent mixing from surface to bottom; (2) light for photosynthesis being limited in the water column; and (3) macrophyte beds composed of dense stands of emergent grasses that retard lateral exchanges.

[29] CO_2 concentrations in the Amazon R. remained at least twofold higher than lake averages in each of the hydrological phases. During rising water, concentrations in L. Curuai increased with river inflow from the main eastern channels. However, during high water, western inflowing channels discharged water from the Amazon R. into littoral regions with CO_2 levels higher than the Amazon R. In this case, the biological processes associated with littoral regions likely influenced high CO_2 levels.

[30] *Richey et al.* [2002] observed CO_2 concentrations in the Amazon R. floodplain ranging from 97 to 1,445 μM. Concentration of CO_2 in the floodplain lakes decreased in downstream reaches, averaging 463 ± 335 μM in the upstream reach between Vargen Grande and Itapeua, where a scroll-bar topography produces mostly long narrow lakes, to 207 ± 138 μM in the downstream reach between São José do Amatari and Óbidos, where a wide floodplain allows the dominance of large shallow lakes.

[31] Our annual average estimate for L. Curuai obtained from all samples was 125 ± 107 μM and falls within the range reported for the downstream reach [*Richey et al.*, 2002]. Longer residence times in larger lakes increases the chances of a more complete decay of organic matter within the lake before carbon is lost by outflow to the main stem. Additionally, shallow lakes with larger open-water areas exposed to wind represent greater potential for aquatic CO_2 evasion. These attributes apply to large floodplain lakes that are more abundant in the downstream reach [*Sippel et al.*, 1992] and may explain their lower mean CO_2 concentration. Given the high spatial variability in these downstream lakes, adequate spatial and temporal sampling is required to determine representative CO_2 concentrations.

[32] Measurements of dissolved CO_2 available from other inland waters in tropical South America are based on regional surveys or occasionally on seasonal or multiyear sampling. In shallow lakes of the Pantanal wetland, median dissolved CO_2 concentrations are about 100 μM with a range from near 0 to 280 μM [*Hamilton et al.*, 1995]. Most of the tropical lakes surveyed by *Kosten et al.* [2010] were supersaturated with values up to about 164 μM. In a shallow interfluvial wetland near the upper Negro River, dissolved CO_2 concentrations obtained over a year averaged 390 μM with standard deviation of 213 μM [*Belger et al.*, 2010]. In Balbina Reservoir on the Uatumã R. in central Brazil, concentrations of dissolved CO_2 in surface waters ranged from 42 to 180 μM during a year of sampling [*Kemenes et al.*, 2011]. *Roland et al.* [2010] reported CO_2 concentrations from Manso and Funil reservoirs, located in the cerrado of Brazil, ranged from 13 to 90 μM in the dry season and from 10 to 100 μM in the rainy season. Collections from the epilimnion at a representative station in Petit Saut Reservoir (French Guiana) ranged from 4 to 773 μM over a multiyear period [*Abril et al.*, 2005].

[33] Based on eddy covariance (EC) measurements *Jonsson et al.* [2008] have demonstrated that conservative estimates are produced using the widely adopted *Cole and Caraco* [1998] model and suggested another wind-based regression. In a reanalysis of the *Jonsson et al.* [2008] data, *MacIntyre et al.* [2010] demonstrated the additional dependence of k_{600} on buoyancy flux and the applicability of the surface renewal model as a mechanistic approach to use in lakes. $k_{600,\ EC}$ computed in this study are almost twice as high as those computed following *Cole and Caraco* [1998]. Estimates of $k_{600,\ SR(zAML\ =\ z\ 0.5\ m)}$ were essentially identical to $k_{600,\ EC}$, which implies that the coefficient c_1 we used applies for the case of a shallow mixing depth. In the absence of actual z_{AML} measurements, our analysis demonstrates the approximate seasonal ranges for $k_{600,\ SR}$ are likely to vary for L. Curuai: 50% during high water, when z_{AML} undergoes larger diel variations; 30% during midstage; and 4% during low water. However, additional effort is required to understand controls on the coefficient, c_1.

[34] During periods with winds sustained above 5 m s^{-1}, with significant wave heights exceeding ~30 cm, *Wanninkhof* [1992] provides better estimates of k_{600} than estimates based on computing turbulence with a surface energy budget (S. MacIntyre, unpublished data, 2010). However, his equation underestimates k_{600} for winds less than 5 m s^{-1}. Given the large size of L. Curuai and the potential for significant wave development, we have computed k_{600} using *Wanninkhof* [1992] for the periods with winds sustained above 5 m s^{-1} for longer than one hour. Such situations occurred about 24% of the time in the four hydrological phases, and k_{600} estimates during those periods were on average 26, 47, and 29% greater than estimates of $k_{600,\ SR(zAML\ =\ z\ mean)}$ during receding, high, and rising water, respectively. At low water the active mixing layer remained shallow, due to constraints of reduced lake depth and high turbidity, and estimates of k_{600} following *Wanninkhof* [1992] were on average 5% lower than estimates of $k_{600,\ SR(zAML\ =\ z\ mean)}$.

[35] The gas exchange coefficients based on *Cole and Caraco*'s [1998] wind-based model and those computed following *MacIntyre et al.* [2010] are two and four times higher, respectively, than the conservative value (k = 2.7 ± 1.0 cm hr^{-1}) used for a regional assessment of rivers and floodplain environments [*Richey et al.*, 2002]. Therefore, it is likely that outgassing of CO_2 from lakes in the lower Amazon floodplain is at least two to four times higher than previously estimated. Furthermore, *Alin et al.* [2011] reported gas exchange coefficients for flowing waters, including large rivers, in the Amazon basin that are similar to those we calculated.

[36] *Richey et al.* [2002] estimated a rate of outgassing of CO_2 from rivers and wetlands of the central Amazon basin, when converted to a daily rate, of 190 ± 55 mmol CO_2 m^{-2} d^{-1}. We estimate mean (±standard deviation) fluxes from open-water in L. Curuai to the atmosphere of 244 ± 15, 348 ± 13, 371 ± 23, and 364 ± 20 mmol CO_2 m^{-2} d^{-1} during receding, low, rising, and high water, respectively. The error associated with these values reflects, for each hydrological phase, the spatial variation in CO_2 concentration in L. Curuai, a likely range in atmospheric CO_2 levels and temporal variations in k_{EC} within the 10-day periods. We used these variations in a Monte Carlo error analysis to determine the variability in areal evasion estimates. These values would be higher if the likely increased concentrations at the air-water interface resulting from nocturnal respiration and mixing were included [*Crill et al.*, 1988; *Åberg et al.*, 2010; *Laurion et al.*, 2010].

[37] The annual water level oscillations affect the dynamics of CO_2 evasion from Amazon floodplains, and predictable biological response to fairly regular hydrological seasonality is expected. However, inter-annual variation in river discharge and annual variability in seasonal timing of peak and minimum stages may cause variations not captured

by a one year study. The use of autonomous CO_2 sensors [e.g., *Lynch et al.*, 2010] and thermistor chains would produce valuable time series and detect important episodic events for further understanding of CO_2 emission from the Amazon floodplain. Additionally, this study focused on the open-water environments of L. Curuai, which account for about 72%, 63%, and 65% of the total flooded area of this floodplain during low, medium (receding and rising), and high water stages, respectively. In order to appraise total aquatic CO_2 evasion additional measurements would be needed from flooded vegetated environments.

6. Conclusions

[38] The open-water environment of large floodplain lakes has high spatial variability in CO_2 concentration with higher concentrations in the littoral and at locations influenced by biological processes and incoming Amazon R. water. Based on results from this study, CO_2 evasion from large lakes in the lower Amazon floodplain will be at least two to four times higher than estimated in current regional calculations. The effects of turbulence induced by wind-mixing and convective cooling, morphology, water level change, habitat type and habitat inundation status, and lake metabolism are all important factors that determine the variations on biogenic gas production and emission rates. Ongoing development of coupled models of lake inundation hydrology, hydrodynamics and biogeochemistry will offer the spatial-temporal resolution needed for resolving carbon dioxide emissions, and the other fluxes of carbon within floodplain ecosystems.

[39] **Acknowledgments.** We are grateful for the funds for the field campaigns granted by Fundação de Amparo à Pesquisa do Estado de São Paulo (FAPESP) (2003/06999–8). Meteorological buoy was funded by Conselho Nacional de Desenvolvimento Científico e Tecnológico (55.0301/02–0) and FAPESP (2002/09911–1). We thank the support provided by the NASA LBA-ECO and Rede GEOMA programs. During the period of manuscript preparation, C. Rudorff was funded by the Ministry of Education of Brazil through a CAPES/Fulbright Award (1705-07-5). Funding was also provided by U.S. National Science Foundation Division of Environmental Biology (grants 0640953 and 0919603). We thank Waldeir Amaral Vilela for his technical assistance.

References

Åberg, J., M. Jansson, and A. Jonsson (2010), The importance of water temperature and thermal stratification dynamics for temporal variation of surface water CO_2 in a boreal lake, *J. Geophys. Res.*, *115*, G02024, doi:10.1029/2009JG001085.

Abril, G., F. Guérin, S. Richard, R. Delmas, C. Galy Lacaux, P. Gosse, A. Tremplay, L. Varfalvy, M. A. Dos Santos, and B. Matvienko (2005), Carbon dioxide and methane emissions and carbon budget of a 10-year old tropical reservoir (Petit Saut, French Guiana), *Global Biogeochem. Cycles*, *19*, GB4007, doi:10.1029/2005GB002457.

Alin, S. R., M. F. F. L. Rasera, C. I. Salimon, J. E. Richey, G. W. Holtgrieve, A. V. Krusche, and A. Snidvongs (2011), Physical controls on carbon dioxide transfer velocity and flux in low-gradient river systems and implications for regional carbon budgets, *J. Geophys. Res.*, *116*, G01009, doi:10.1029/2010JG001398.

Amorocho, J., and J. J. DeVries (1980), A new evaluation of the wind stress coefficient over water surfaces, *J. Geophys. Res.*, *85*, 433–442, doi:10.1029/JC085iC01p00433.

Anselin, L. (1995), Local Indicators of Spatial Association—LISA, *Geogr. Anal.*, *27*, 93–115, doi:10.1111/j.1538-4632.1995.tb00338.x.

Barbosa, C. C. F., E. M. L. M. Novo, J. M. Melack, R. M. Freitas, and W. P. Filho (2006), Metodologia de análise da dinâmica de área e volume inundável: O exemplo do várzea do Lago Grande de Curuai, *Rev. Bras. Cartografia*, *58*, 200–210.

Barbosa, C. C. F., E. M. L. M. Novo, J. M. Melack, M. Gastil-Buhl, and W. P. Filho (2010), Geospatial analysis of spatiotemporal patterns of pH, total suspended sediment and chlorophyll-a on the Amazon floodplain, *Limnology*, *11*, 155–166, doi:10.1007/s10201-009-0305-5.

Belger, L., B. R. Forsberg, and J. M. Melack (2010), Carbon dioxide and methane emissions from interfluvial wetlands in the upper Negro River basin, Brazil, *Biogeochemistry*, doi:10.1007/s10533-010-9536-0.

Bonnet, M. P., et al. (2008), Floodplain hydrology in an Amazon floodplain lake (Lago Grande de Curuaí), *J. Hydrol.*, *349*, 18–30, doi:10.1016/j.jhydrol.2007.10.055.

Buhmann, M. D. (2003), *Radial Basis Functions: Theory and Implementations*, Cambridge Univ. Press, Cambridge, U. K, doi:10.1017/CBO9780511543241.

Butler, J. N. (1992), *Carbon Dioxide Equilibria and Their Applications*, Addison-Wesley, Reading, Mass.

Cole, J. J., and N. F. Caraco (1998), Atmospheric exchange of carbon dioxide in a low-wind oligotrophic lake measured by the addition of SF_6, *Limnol. Oceanogr.*, *43*, 647–656, doi:10.4319/lo.1998.43.4.0647.

Crill, P., K. B. Bartlett, J. D. Wilson, D. K. Sebacker, R. C. Harriss, J. M. Melack, S. MacIntyre, L. Lesack, and L. Smith-Morrill (1988), Tropho-spheric methane from an Amazon floodplain lake, *J. Geophys. Res.*, *93*, 1564–1570, doi:10.1029/JD093iD02p01564.

Engle, D. L., J. M. Melack, R. D. Doyle, and T. R. Fisher (2008), High rates of net primary production and turnover of floating grasses on the Amazon floodplain: Implications for aquatic respiration and regional CO_2 flux, *Global Change Biol.*, *14*, 369–381, doi:10.1111/j.1365-2486.2007.01481.x.

Fitzjarrald, D. R., R. K. Sakai, and O. L. L. de Moraes (2009), LBA-ECO CD-03 Mesoscale Meteorological Data, Santarem Region, Pará, Brazil: 1998–2006, data set, http://daac.ornl.gov, Oak Ridge Natl. Lab. Distrib. Act. Arch. Cent., Oak Ridge, Tenn.

Hamilton, S. K., S. J. Sippel, and J. M. Melack (1995), Oxygen depletion and carbon dioxide and methane production in waters of the Pantanal wetland of Brazil, *Biogeochemistry*, *30*, 115–141, doi:10.1007/BF00002727.

Houghton, R. A., M. Gloor, J. Lloyd, and C. Potter (2009), The regional carbon budget, in *Amazonia and Global Change*, *Geophys. Monogr. Ser*, vol. 186, edited by M. Keller et al., pp. 409–428, AGU, Washington, D. C.

Imberger, J. (1985), The diurnal mixed layer, *Limnol. Oceanogr.*, *30*, 737–770, doi:10.4319/lo.1985.30.4.0737.

Isenogle, S. S. (1985), A laboratory study of gas transfer across an air-water interface, M.S. thesis, Univ. of Southern Calif., Los Angeles.

Jähne, B., K. O. Münnich, R. B. A. Dutzi, W. Huber, and P. Libner (1987), On the parameters influencing air-water gas exchange, *J. Geophys. Res.*, *92*, 1937–1949, doi:10.1029/JC092iC02p01937.

Jellison, R., and J. M. Melack (1993), Meromixis in hypersaline Mono Lake, California. 1. Stratification and vertical mixing during the onset, persistence, and breakdown of meromixis, *Limnol. Oceanogr.*, *38*, 1008–1019, doi:10.4319/lo.1993.38.5.1008.

Jonsson, A., J. Åberg, A. Lindroth, and M. Jansson (2008), Gas transfer rate and CO_2 flux between an unproductive lake and the atmosphere in northern Sweden, *J. Geophys. Res.*, *113*, G04006, doi:10.1029/2008JG000688.

Junk, W. J. (1997), *The Central Amazon Floodplain: Ecology of a Pulsing System*, Springer, Berlin.

Kemenes, A., B. R. Forsberg, and J. M. Melack (2011), CO_2 emissions from a tropical hydroelectric reservoir (Balbina, Brazil). *J. Geophys. Res.*, *116*, G03004, doi:10.1029/2010JG001465.

Koenings, J. P., and J. A. Edmundson (1991), Secchi disk and photometer estimates of light regimes in Alaskan lakes: Effects of yellow color and turbidity, *Limnol. Oceanogr.*, *36*, 91–105, doi:10.4319/lo.1991.36.1.0091.

Kosten, S., F. Roland, D. M. L. da Motta Marques, E. H. Van Nes, N. Mazzeo, L. da S. L. Sternberg, M. Scheffer, and J. J. Cole (2010), Climate-dependent CO_2 emissions from lakes, *Global Biogeochem. Cycles*, *24*, GB2007, doi:10.1029/2009GB003618.

Laurion, I., W. F. Vincent, S. MacIntyre, L. Retamal, C. Dupont, P. Francus, and R. Pienitz (2010), Variability in greenhouse gas emissions from permafrost thaw ponds, *Limnol. Oceanogr.*, *55*, 115–133, doi:10.4319/lo.2010.55.1.0115.

Lombardo, C. P., and M. C. Gregg (1989), Similarity scaling of viscous and thermal dissipation in a convecting surface boundary layer, *J. Geophys. Res.*, *94*, 6273–6284, doi:10.1029/JC094iC05p06273.

Lynch, J. K., C. M. Beatty, M. P. Seidel, L. J. Jungst, and M. D. DeGrandpre (2010), Controls of riverine CO_2 over an annual cycle determined using direct, high temporal resolution pCO_2 measurements, *J. Geophys. Res.*, *115*, G03016, doi:10.1029/2009JG001132.

MacIntyre, S., and J. M. Melack (1984), Vertical mixing in Amazon floodplain lakes, *Verh. Int. Ver. Limnol.*, *22*, 1283–1287.

MacIntyre, S., and J. M. Melack (1988), Frequency and depth of vertical mixing in an Amazon floodplain lake (L. Calado, Brazil), *Verh. Int. Ver. Limnol.*, *23*, 80–85.

MacIntyre, S., R. Wanninkhof, and J. P. Chanton (1995), Trace gas exchange across the air-water interface in freshwaters and costal marine environments, in *Biogenic Trace Gases: Measuring Emissions From Soil and Water*, edited by P. A. Matson and R. C. Harriss, pp. 52–97, Blackwell, Oxford, U. K.

MacIntyre, S., J. P. Fram, P. J. Kushner, N. D. Bettez, W. J. O'Brien, J. E. Hobbie, and G. W. Kling (2009), Climate-related variations in mixing dynamics in an Alaskan arctic lake, *Limnol. Oceanogr.*, *54*, 2401–2417.

MacIntyre, S., A. Jonsson, M. Jansson, J. Åberg, D. E. Turney, and S. Miller (2010), Buoyancy flux, turbulence, and the gas transfer coefficient in a stratified lake, *Geophys. Res. Lett.*, *37*, L24604, doi:10.1029/2010GL044164.

Mayorga, E., A. K. Aufdenkampe, C. A. Masiello, A. V. Krusche, J. I. Hedges, P. D. Quay, J. E. Richey, and T. A. Brown (2005), Young organic matter as a source of carbon dioxide outgassing from Amazonian rivers, *Nature*, *436*, 538–541, doi:10.1038/nature03880.

Melack, J. M., and D. L. Engle (2009), An organic carbon budget for an Amazon floodplain lake, *Verh. Int. Ver. Limnol.*, *30*, 1179–1182.

Melack, J. M., and T. R. Fisher (1983), Diel oxygen variations and their ecological implication in Amazon floodplain lakes, *Arch. Hydrobiol.*, *98*, 422–442.

Melack, J. M., E. M. L. M. Novo, B. R. Forsberg, M. T. F. Piedade, and L. Maurice (2009), Floodplain ecosystem processes, in *Amazonia and Global Change*, *Geophys. Monogr. Ser*, vol. 186, edited by M. Keller et al., pp. 525–541, AGU, Washington, D. C.

Miller, S., M. Goulden, and H. R. da Rocha (2009), LBA-ECO CD-04 Meteorological and Flux Data, km 83 Tower Site, Tapajos National Forest, data set, http://daac.ornl.gov, Oak Ridge Natl. Lab. Distrib. Act. Arch. Cent., Oak Ridge, Tenn.

Moran, P. A. P. (1948), The interpretation of statistical maps, *J. R. Stat. Soc., Ser. B*, *10*, 243–251.

Plummer, L., and E. Busenberg (1982), The solubilities of calcite, aragonite and vaterite in CO_2-H_2O solutions between 0 and 90°C, and an evaluation of the aqueous model for the system $CaCO_3$-CO_2-H_2O, *Geochim. Cosmochim. Acta*, *46*, 1011–1040, doi:10.1016/0016-7037(82)90056-4.

Quay, P. D., D. O. Wilbur, J. E. Richey, J. I. Hedges, A. H. Devol, and R. Victoria (1992), Carbon cycling in the Amazon River: Implications from the ^{13}C compositions of particles and solutes, *Limnol. Oceanogr.*, *37*, 857–871, doi:10.4319/lo.1992.37.4.0857.

Richey, J. E., A. H. Devol, S. C. Wofsy, R. Victoria, and M. N. G. Riberio (1988), Biogenic gases and the oxidation and reduction of carbon in Amazon River and floodplain waters, *Limnol. Oceanogr.*, *33*, 551–561, doi:10.4319/lo.1988.33.4.0551.

Richey, J. E., J. M. Melack, A. K. Aufdenkampe, V. M. Ballester, and L. L. Hess (2002), Outgassing from Amazonian rivers and wetlands as a large tropical source of atmospheric CO_2, *Nature*, *416*, 617–620, doi:10.1038/416617a.

Richey, J. E., A. V. Krusche, M. S. Johnson, H. B. Cunha, and M. V. Ballester (2009), The role of rivers in the regional carbon balance, in *Amazonia and Global Change*, *Geophys. Monogr. Ser*, vol. 186, edited by M. Keller et al., pp. 489–504, AGU, Washington, D. C.

Ripley, B. D. (1981), *Spatial Statistics*, Wiley, New York.

Roland, F., L. O. Vidal, F. S. Pacheco, N. O. Barros, A. Assireu, J. P. H. B. Ometto, A. C. P. Cimbleris, and J. J. Cole (2010), Variability of carbon dioxide flux from tropical (Cerrado) hydroelectric reservoirs, *Aquat. Sci.*, *72*, 283–293, doi:10.1007/s00027-010-0140-0.

Shay, T. J., and M. C. Gregg (1986), Convectively driven turbulent mixing in the upper ocean, *J. Phys. Oceanogr.*, *16*, 1777–1798, doi:10.1175/1520-0485(1986)016<1777:CDTMIT>2.0.CO;2.

Sippel, S. J., S. K. Hamilton, and J. M. Melack (1992), Inundation area and morphometry of lakes on the Amazon River floodplain, Brazil, *Arch. Hydrobiol.*, *123*, 385–400.

Stumm, W., and J. J. Morgan (1996), *Aquatic Chemistry: Chemical Equilibria and Rates in Natural Waters*, Wiley-Interscience, New York.

Waichman, A. V. (1996), Autotrophic carbon sources for heterotrophic bacterioplankton in a floodplain lake of central Amazon, *Hydrobiologia*, *341*, 27–36, doi:10.1007/BF00012300.

Wanninkhof, R. (1992), Relationship between wind speed and gas exchange over the ocean, *J. Geophys. Res.*, *97*, 7373–7382, doi:10.1029/92JC00188.

Zappa, C. J., W. R. McGillis, P. A. Raymond, J. B. Edson, E. J. Hintsa, H. J. Zemmelink, J. W. H. Dacey, and D. T. Ho (2007), Environmental turbulent mixing controls on air-water gas exchange in marine and aquatic systems, *Geophys. Res. Lett.*, *34*, L10601, doi:10.1029/2006GL028790.

C. C. F. Barbosa and E. M. L. M. Novo, Coordenação de Observação da Terra, Instituto Nacional de Pesquisas Espaciais, São José dos Campos, 12227-010 São Paulo, Brazil.

S. MacIntyre, Marine Science Institute, University of California, Santa Barbara, CA 93106, USA.

J. M. Melack and C. M. Rudorff, Bren School of Environmental Science and Management, University of California, Santa Barbara, CA 93106, USA. (cmr@bren.ucsb.edu)